

# Two Higgs bosons near 125 GeV in the complex NMSSM and the LHC Run-I data

Stefano Moretti<sup>a</sup> and Shoaib Munir<sup>b</sup>

<sup>a</sup>*School of Physics & Astronomy,  
University of Southampton, Southampton SO17 1BJ, UK*

<sup>b</sup>*Asia Pacific Center for Theoretical Physics, San 31, Hyoja-dong,  
Nam-gu, Pohang 790-784, Republic of Korea*

s.moretti@soton.ac.uk, s.munir@apctp.org

## Abstract

We analyse the impact of explicit CP-violation in the Higgs sector of the Next-to-Minimal Supersymmetric Standard Model (NMSSM) on its consistency with the Higgs boson data from the Large Hadron Collider (LHC). Through detailed scans of the parameter space of the complex NMSSM for certain fixed values of one of its CP-violating (CPV) phases, we obtain a large number of points corresponding to five phenomenologically relevant scenarios containing  $\sim 125$  GeV Higgs boson(s). We focus, in particular, on the scenarios where the visible peaks in the experimental samples can actually be explained by two nearly mass-degenerate neutral Higgs boson states. We find that some points corresponding to these scenarios give an overall slightly improved fit to the data, more so for non-zero values of the CPV phase, compared to the scenarios containing a single Higgs boson near 125 GeV.

# 1 Introduction

The Higgs sector of the NMSSM [1] (see, e.g., [2, 3] for reviews) contains two additional neutral mass eigenstates besides the three of the Minimal Supersymmetric Standard Model (MSSM). This is due to the presence of a Higgs singlet superfield besides the two doublet superfields of the MSSM. When all the parameters in the Higgs and sfermion sectors of the NMSSM are real, one of these new Higgs states is a scalar and the other a pseudoscalar. Hence, in total three scalars,  $H_{1,2,3}$ , and two pseudoscalars,  $A_{1,2}$ , make up the neutral Higgs boson content of the model. This extended Higgs sector of the NMSSM boasts some unique phenomenological possibilities, which are either precluded or experimentally ruled out in the MSSM. For example, in the NMSSM either of the two lightest CP-even Higgs bosons,  $H_1$  or  $H_2$ , can play the role of the  $\sim 125$  GeV Standard Model (SM)-like Higgs boson,  $H_{\text{obs}}$ , observed at the LHC [4, 5, 6].

Of particular interest in the NMSSM is the possibility that the SM-like Higgs boson can obtain a large tree-level mass in a *natural* way, i.e., without requiring large radiative corrections from the supersymmetric sectors. This happens in a specific region of the parameter space, which we refer to as the natural NMSSM, where there is a significant singlet-doublet mixing and the  $H_{\text{obs}}$  is typically  $H_2$ . This scenario was used to explain [7] the enhancement in the  $H_{\text{obs}} \rightarrow \gamma\gamma$  channel in the early LHC data. However, when the singlet-doublet mixing is too large, the properties of  $H_2$  can deviate appreciably from an exact SM-like behaviour, resulting in a reduction of its fermionic partial decay widths. An alternative possibility in a very similar parameter space region is that of both  $H_1$  and  $H_2$  simultaneously having masses near 125 GeV [8, 9]. In that case, the observed excess at the LHC could actually be due to a superposition of these two states, when their individual signal peaks cannot be resolved separately. One of these two Higgs bosons, typically  $H_1$ , is the singlet-like neutral state. Moreover, in [10] it was noted that the lighter of the two pseudoscalars,  $A_1$ , when it is singlet-like, could also be nearly mass-degenerate with a SM-like  $H_1$  near 125 GeV, instead of or even along with the  $H_2$ . However, such a pseudoscalar can only contribute visibly to the measured signal strength near 125 GeV if it is produced in association with a  $b\bar{b}$  pair.

One of the most important yet unresolved issues in particle physics is that of the observed matter-antimatter asymmetry in the universe. A plausible explanation for this asymmetry is electroweak (EW) baryogenesis [11]. The necessary conditions for successful EW baryogenesis include the following [12]: (1) baryon number violation, (2) CP-violation and (3) departure from equilibrium at the critical temperature of the EW symmetry breaking (EWSB) phase transition, implying that it is strongly first order. In the SM, a strongly first order EW phase transition is not possible given the measured mass of the Higgs boson at the LHC. Besides, the only source of CP-violation in the SM, the Cabibbo-Kobayashi-Maskawa matrix, is insufficient. Therefore, beyond the SM, a variety of sources of CP-violation have been proposed in the literature (for a review, see [13] and references therein). In the context of supersymmetry (SUSY), a strongly first order phase transition is possible in the MSSM only if the lightest stop has a mass below that of the top quark. This possibility has now been ruled out by SUSY searches at the LHC [14]. Also, the MSSM Higgs sector does not violate CP at the tree level but does so only at higher orders [15, 16, 17]. The CPV phases, transmitted radiatively to the Higgs sector via couplings to the sfermions, are tightly constrained by the measurements of fermion electric dipole moments (EDMs) [18]. However, these EDM constraints can be relaxed under certain conditions [16, 19, 20].

The NMSSM has been shown to accommodate a strongly first order EW phase transition without a light stop [21]. Additionally, in this model, CP-violation can be invoked explicitly in the Higgs sector even at the tree level by assuming the Higgs self-couplings,  $\lambda$  and  $\kappa$ , to be complex. Beyond the Born approximation, the phase of the SUSY-breaking Higgs-sfermion-sfermion couplings,  $A_{\tilde{f}}$ , where  $f$  denotes a SM fermion, is also induced in the Higgs sector, as in the MSSM. In the presence

of the associated complex phases, the five neutral Higgs bosons are CP-indefinite states, due to the mixing between the scalar and pseudoscalar interaction eigenstates. CPV phases can therefore influence the phenomenology of the NMSSM Higgs bosons by, e.g., modifying their mass spectrum as well as their production and decay rates [22], similarly to the MSSM [23]. The impact of these phases in the complex NMSSM (cNMSSM), i.e., the CPV NMSSM, on the necessary conditions for successful EW phase transition was also studied some time ago [24]. The consistency of scenarios yielding the correct baryon asymmetry with the LHC Higgs boson data still remains to be studied in depth, though. However, even leaving aside these considerations, the possibly distinct phenomenological scenarios that the cNMSSM can yield make it a particularly interesting model for exploration at the Run-II of the LHC.

The cNMSSM has therefore been the subject of several studies recently and, in particular, some important theoretical developments have been made in the model. The dominant 1-loop corrections to the neutral Higgs sector from the (s)quark and gauge sectors were studied in [25, 26], in the renormalisation group equations-improved effective potential approach. The corrections from the gaugino sector were included in [27] and, more inclusively, recently in [28]. In the Feynman diagrammatic approach, the complete 1-loop Higgs mass matrix was derived in [29] and the  $\mathcal{O}(\alpha_t\alpha_s)$  contributions to it were calculated in [30]. As far as the phenomenology of the Higgs bosons in the cNMSSM is concerned, the consistency of several CPV scenarios with the early results on the  $H_{\text{obs}}$  from the LHC data was studied in detail in [29, 22]. Another distinct phenomenological scenario, possible only for non-zero CPV phases, has also been studied in [27].

The CMS and ATLAS collaborations have recently updated their measurements of the  $H_{\text{obs}}$  signal rates in the  $\tau^+\tau^-$  and  $b\bar{b}$  channels [31, 32]. The fact that these rates also tend to favour a SM-like  $H_{\text{obs}}$  is increasingly jeopardising the above mentioned natural NMSSM scenario with large singlet-doublet mixing but only with one Higgs boson, either  $H_1$  or  $H_2$ , around 125 GeV. This makes the scenario with both  $H_1$  and  $H_2$  contributing to the observed  $\sim 125$  GeV signal all the more important, since it may potentially satisfy better the current Higgs boson data while still leaving plenty of room for new physics. In case of the cNMSSM, since the five neutral Higgs bosons are CP-mixed states, the scenario with mass-degenerate  $H_1$  and  $H_2$  can entail both the corresponding possibilities in the real NMSSM (rNMSSM), i.e., mass-degenerate  $H_1$ ,  $H_2$  or  $H_1/H_2$ ,  $A_1$ .

In this study we therefore analyse and compare the prospects for scenarios with two mass-degenerate Higgs bosons against those with a single Higgs boson near 125 GeV in the  $Z_3$ -invariant cNMSSM. We perform scans of the relevant parameter space [8] of the model using the public program NMSSMCALC [33] to search for all possible  $\sim 125$  GeV Higgs boson scenarios, with the CPV phase of the coupling  $\kappa$  set to five different values, including  $0^\circ$  - the rNMSSM limit - in each case. The condition for mass-degeneracy between two Higgs bosons is imposed by requiring them to lie within 2.5 GeV of each other, which is consistent with the current mass resolution of the LHC [34], taking into account the uncertainties in the theoretical mass prediction. We then use fits to the Higgs boson data from the LHC Run-I, both with  $\sqrt{s} = 7$  TeV and  $\sqrt{s} = 8$  TeV, as well as from the Tevatron, performed using the program HiggsSignals [35], as the sole criterion for comparing the present likelihood of each of these scenarios. We also discuss how these mass-degenerate Higgs bosons can be identified at the LHC based on the signal rate double ratios introduced in [36].

The article is organised as follows. In the next section we will briefly revisit the Higgs sector of the cNMSSM. In section 3 we will provide details of our numerical scans and our procedure for fitting the model predictions for the Higgs boson(s) to the LHC data. In section 4 we will discuss the results of our analysis and in section 5 we will present our conclusions.

## 2 The Higgs sector of the cNMSSM

The NMSSM contains a singlet Higgs superfield,  $\widehat{S}$ , besides the two  $SU(2)_L$  doublet superfields,

$$\widehat{H}_u = \begin{pmatrix} \widehat{H}_u^+ \\ \widehat{H}_u^0 \end{pmatrix}, \quad \widehat{H}_d = \begin{pmatrix} \widehat{H}_d^0 \\ \widehat{H}_d^- \end{pmatrix}, \quad (1)$$

of the MSSM. The superpotential of the NMSSM is written as

$$W_{\text{NMSSM}} = \text{MSSM Yukawa terms} + \lambda \widehat{S} \widehat{H}_u \widehat{H}_d + \frac{\kappa}{3} \widehat{S}^3, \quad (2)$$

where  $\lambda$  and  $\kappa$  are dimensionless Yukawa couplings. This superpotential is scale invariant, since the term  $\mu \widehat{H}_u \widehat{H}_d$  appearing in the MSSM superpotential has been removed by imposing a discrete  $Z_3$  symmetry. In this model, an effective  $\mu$ -term,  $\mu_{\text{eff}} = \lambda s$ , is instead generated when the singlet field acquires a vacuum expectation value (VEV),  $s$ , which is naturally of the order of the SUSY-breaking scale.

The tree-level Higgs potential of the NMSSM, obtained from the superpotential in eq. (2), is written in terms of the neutral scalar components of the Higgs superfields,  $H_u$ ,  $H_d$ , and  $S$ , as

$$\begin{aligned} V_0 &= |\lambda (H_u^+ H_d^- - H_u^0 H_d^0) + \kappa S^2|^2 \\ &+ (m_{H_u}^2 + |\lambda S|^2) (|H_u^0|^2 + |H_u^+|^2) + (m_{H_d}^2 + |\lambda S|^2) (|H_d^0|^2 + |H_d^-|^2) \\ &+ \frac{g^2}{4} (|H_u^0|^2 + |H_u^+|^2 - |H_d^0|^2 - |H_d^-|^2)^2 + \frac{g_2^2}{2} |H_u^+ H_d^{0*} + H_u^0 H_d^{-*}|^2 \\ &+ m_S^2 |S|^2 + (\lambda A_\lambda (H_u^+ H_d^- - H_u^0 H_d^0) S + \frac{1}{3} \kappa A_\kappa S^3 + \text{h.c.}), \end{aligned} \quad (3)$$

where  $g^2 \equiv \frac{g_1^2 + g_2^2}{2}$ , with  $g_1$  and  $g_2$  being the  $U(1)_Y$  and  $SU(2)_L$  gauge couplings, respectively, and  $A_\lambda$  and  $A_\kappa$  are the soft SUSY-breaking Higgs trilinear couplings. The scalar fields  $H_u$ ,  $H_d$  and  $S$  are developed around their respective VEVs,  $v_u$ ,  $v_d$  and  $s$ , as

$$\begin{aligned} H_d^0 &= \begin{pmatrix} \frac{1}{\sqrt{2}} (v_d + H_{dR} + iH_{dI}) \\ H_d^- \end{pmatrix}, \\ H_u^0 &= e^{i\theta} \begin{pmatrix} H_u^+ \\ \frac{1}{\sqrt{2}} (v_u + H_{uR} + iH_{uI}) \end{pmatrix}, \\ S &= \frac{e^{i\varphi}}{\sqrt{2}} (s + S_R + iS_I). \end{aligned} \quad (4)$$

The Higgs coupling parameters appearing in the potential in eq. (3) can very well be complex, implying  $\lambda \equiv |\lambda| e^{i\phi_\lambda}$ ,  $\kappa \equiv |\kappa| e^{i\phi_\kappa}$ ,  $A_\lambda \equiv |A_\lambda| e^{i\phi_{A_\lambda}}$  and  $A_\kappa \equiv |A_\kappa| e^{i\phi_{A_\kappa}}$ . As a result, the  $V_0$ , evaluated at the vacuum, contains the phase combinations

$$\phi'_\lambda \equiv \phi_\lambda + \theta + \varphi, \quad \phi'_\kappa \equiv \phi_\kappa + 3\varphi, \quad \phi'_\lambda + \phi_{A_\lambda} \quad \text{and} \quad \phi'_\kappa + \phi_{A_\kappa}. \quad (5)$$

For correct EWSB, the Higgs potential should have a minimum at non-vanishing  $v_u$ ,  $v_d$  and  $s$ , which is ensured by requiring

$$\left\langle \frac{\delta V_0}{\delta \Phi} \right\rangle = 0 \quad \text{for} \quad \Phi = H_{dR}, H_{uR}, S_R, H_{dI}, H_{uI}, S_I. \quad (6)$$

Through the above minimisation conditions the phase combinations  $\phi'_\lambda + \phi_{A_\lambda}$  and  $\phi'_\kappa + \phi_{A_\kappa}$  can be determined up to a twofold ambiguity by  $\phi'_\lambda - \phi'_\kappa$ . Thus,  $\phi'_\lambda - \phi'_\kappa$  is the only physical CP phase appearing in the NMSSM Higgs sector at the tree level. Also, using these conditions, the soft mass parameters  $m_{H_u}^2$ ,  $m_{H_d}^2$  and  $m_S^2$  can be traded for the corresponding Higgs field VEVs.

The neutral Higgs mass matrix is obtained by taking the second derivative of the  $V_0$  evaluated at the vacuum. This  $5 \times 5$  matrix,  $\mathcal{M}_0^2$ , in the  $\mathbf{H}^T = (H_{dR}, H_{uR}, S_R, H_I, S_I)$  basis, from which the massless Nambu-Goldstone mode has been rotated away, can be diagonalised using an orthogonal matrix,  $O$ , as  $O^T \mathcal{M}_0^2 O = \text{diag}(m_{H_1}^2, m_{H_2}^2, m_{H_3}^2, m_{H_4}^2, m_{H_5}^2)$ . This yields the physical tree-level masses corresponding to the five mass eigenstates,

$$(H_1, H_2, H_3, H_4, H_5)_a^T = O_{ai} (H_{dR}, H_{uR}, S_R, H_I, S_I)_i^T, \quad (7)$$

such that  $m_{H_1}^2 \leq m_{H_2}^2 \leq m_{H_3}^2 \leq m_{H_4}^2 \leq m_{H_5}^2$ . The elements,  $O_{ai}$ , of the mixing matrix then govern the couplings of the Higgs bosons to all the particles in the model.

The tree-level Higgs mass matrix is subject to higher order corrections from the SM fermions, from the gauge and chargino/neutralino sectors and the Higgs sector itself, as well as from the sfermion sector, in the case of which they are dominated by the stop contributions. Upon the inclusion of these corrections,  $\Delta\mathcal{M}^2$ , the Higgs mass matrix gets modified, so that

$$\mathcal{M}_H^2 = \mathcal{M}_0^2 + \Delta\mathcal{M}^2. \quad (8)$$

Explicit expressions for  $\mathcal{M}_0^2$  as well as for  $\Delta\mathcal{M}^2$  can be found in [29, 27, 28]. Thus, beyond the Born approximation, the CPV phases of the gaugino mass parameters,  $M_{1,2}$ , and of  $A_{\tilde{f}}$  are also radiatively induced in the Higgs sector of the NMSSM.

Therefore, when studying the phenomenology of the Higgs bosons, one needs to take into account also the parameters from the other sectors of the model. However, the most general NMSSM contains more than 130 parameters at the EW scale. Assuming the matrices for the sfermion masses and for the trilinear scalar couplings to be diagonal considerably reduces the number of free parameters. One can further exploit the fact, mentioned above, that the corrections to the Higgs boson masses from the sfermions are largely dominated by the stop sector. For our numerical analysis in the following sections, we will thus impose the following supergravity-inspired universality conditions on the model parameters at the EW scale:

$$\begin{aligned} M_0 &\equiv M_{Q_{1,2,3}} = M_{U_{1,2,3}} = M_{D_{1,2,3}} = M_{L_{1,2,3}} = M_{E_{1,2,3}}, \\ M_{1/2} &\equiv 2M_1 = M_2 = \frac{1}{3}M_3, \\ A_0 &\equiv A_{\tilde{t}} = A_{\tilde{b}} = A_{\tilde{\tau}}, \end{aligned} \quad (9)$$

where  $M_{Q_{1,2,3}}^2$ ,  $M_{U_{1,2,3}}^2$ ,  $M_{D_{1,2,3}}^2$ ,  $M_{L_{1,2,3}}^2$  and  $M_{E_{1,2,3}}^2$  are the squared soft masses of the sfermions,  $M_{1,2,3}$  those of the gauginos and  $A_{\tilde{t},\tilde{b},\tilde{\tau}}$  the soft trilinear couplings. Altogether, the input parameters of the cNMSSM then include

$$M_0, |M_{1/2}|, |A_0|, \tan\beta (\equiv v_u/v_d), |\lambda|, |\kappa|, \mu_{\text{eff}}, |A_\lambda|, |A_\kappa|, \theta_{1/2}, \theta_{\tilde{f}}, \phi'_\lambda \text{ and } \phi'_\kappa,$$

where  $\theta_{1/2}$  and  $\theta_{\tilde{f}}$  are the phases of the unified parameters  $M_{1/2}$  and  $A_0$ , respectively.

### 3 Numerical analysis

As noted in the Introduction, non-zero CPV phases can modify appreciably the masses and decay widths of the neutral Higgs bosons compared to the CP-conserving case for a given set of the

remaining free parameters. In the case of the  $H_{\text{obs}}$  candidate in the model, whether  $H_1$  or  $H_2$  or even  $H_3$ , the CPV phases are thus strongly constrained by the LHC mass and signal rate measurements. This was analysed in detail in [22], where the scenarios with mass-degenerate Higgs bosons were, however, not taken into account. In the present study we thus test whether the said modifications in the Higgs boson properties with non-zero values of the phase  $\phi'_\kappa$  (by which we imply  $\phi_\kappa$ , which is the actual physically meaningful phase, since  $\varphi$  can be absorbed into  $\phi'_\kappa$  by a field re-definition) can lead to a relatively improved consistency with the experimental data.

The reason for choosing  $\phi'_\kappa$  as the only variable phase, while setting  $\theta_{1/2}$ ,  $\theta_{\tilde{f}}$  and  $\phi'_\lambda$  to  $0^\circ$ , is that it is virtually unconstrained by the measurements of fermionic EDMs [26, 29]. Furthermore, our aim here is to analyse the scenarios with a generic CPV phase and compare them with the rNMSSM limit rather than measuring the effect of any of the individual phases. Note however that, since only the difference  $\phi'_\lambda - \phi'_\kappa$  enters the Higgs mass matrix at the tree level, the impact of a variation in  $\phi'_\lambda$  is also quantified by that due to the variation in  $\phi'_\kappa$  at this level. At higher orders though, a variation in  $\phi'_\lambda$  has an impact on the sfermion and neutralino/chargino sectors which is independent of  $\phi'_\kappa$ .

In our numerical analysis, we used the program NMSSMCALC-v1.03 [33] for computing the Higgs boson mass spectrum and decay branching ratios (BRs) for a given model input point. The public distribution of NMSSMCALC contains two separate packages, one for the rNMSSM only and the other for the cNMSSM. Some supersymmetric corrections to the Higgs boson decay widths are currently only available in the rNMSSM and hence are not included in the cNMSSM package. For consistency among our rNMSSM and cNMSSM results, we therefore set  $\phi_\kappa = 0^\circ$  in the cNMSSM package for the rNMSSM case instead of using the dedicated rNMSSM package. Furthermore, using the cNMSSM code also for the rNMSSM limit makes it convenient to draw a one-on-one correspondence between the  $\phi_\kappa = 0^\circ$  case and each of the  $\phi_\kappa > 0^\circ$  cases in a given scenario. This is because in the cNMSSM package, even in the rNMSSM limit, the five neutral Higgs bosons are ordered by their masses and not separated on the basis of their CP-identities. Thus, the scenario with mass-degenerate  $H_1$ ,  $H_2$ , which we will henceforth refer to as the  $H_{\text{obs}} = H_1 + H_2$  scenario, takes into account both the  $\sim 125$  GeV  $H_1$ ,  $H_2$  as well as the  $\sim 125$  GeV  $H_1$ ,  $A_1$  solutions of the rNMSSM without distinguishing between them. If one, conversely, uses the rNMSSM package, these two scenarios ought to be considered separately. The same is true also for the  $H_{\text{obs}} = H_2 + H_3$  scenario, wherein  $H_2$ ,  $H_3$  are mass-degenerate.

The program NMSSMCALC allows one the option to include only the complete 1-loop contributions in the Higgs mass matrix or to add also the 2-loop  $\mathcal{O}(\alpha_t\alpha_s)$  corrections to it. For our analysis, in order for better theoretical precision, we evaluated the Higgs boson masses at the 2-loop level. In the NMSSMCALC input, one also needs to choose between the modified dimensional regularisation ( $\overline{\text{DR}}$ ) and on-shell renormalisation schemes for calculating contributions from the top/stop sector in the program. We opted for the  $\overline{\text{DR}}$  scheme for each scenario. Note though that further inclusion of  $\mathcal{O}(\alpha_b\alpha_s)$ ,  $\mathcal{O}(\alpha_t + \alpha_b + \alpha_\tau)^2$  and the recently calculated NMSSM-specific  $\mathcal{O}(\alpha_\lambda + \alpha_\kappa)^2$  2-loop corrections [37] in NMSSMCALC may have a non-negligible impact on the Higgs boson masses and observables [38]. We, however, maintain that such contributions will only result in a slight shifting of the parameter configurations yielding solutions of our interest here, but our overall results and conclusions should still remain valid.

We performed six sets of scans of the cNMSSM parameter space by linking NMSSMCALC with the MultiNest-v2.18 [39] package. MultiNest performs a multimodal sampling of a theoretical model's parameter space based on Bayesian evidence estimation. However, we use this package not for drawing Bayesian inferences about the various NMSSM scenarios considered but simply to avoid a completely random sampling of the 9-dimensional model parameter space. In the program, we therefore defined a Gaussian likelihood function for the  $H_{\text{obs}}$  in a given scan, assuming the

Parameter	Natural NMSSM range	Parameter	Low- $\lambda$ -NMSSM range
$M_0$ (GeV)	200 – 2000	$M_0$ (GeV)	200 – 4000
$M_{1/2}$ (GeV)	100 – 1000	$M_{1/2}$ (GeV)	100 – 2000
$A_0$ (GeV)	–3000 – 0	$A_0$ (GeV)	–7000 – 0
$\tan \beta$	1 – 8	$\tan \beta$	5 – 45
$\lambda$	0.4 – 0.7	$\lambda$	0.001 – 0.4
$\kappa$	0.3 – 0.6	$\kappa$	0.001 – 0.3
$\mu_{\text{eff}}$ (GeV)	100 – 300	$\mu_{\text{eff}}$ (GeV)	100 – 2000
$A_\lambda$ (GeV)	–1000 – 1000	$A_\lambda$ (GeV)	–1000 – 4000
$A_\kappa$ (GeV)	–1000 – 1000	$A_\kappa$ (GeV)	–4000 – 1000

(a)

(b)

Table 1: Ranges of the NMSSM parameters scanned, with fixed  $\phi_\kappa$ , for (a) each  $H_{\text{obs}}$  scenario in the natural NMSSM and (b) the low- $\lambda$ -NMSSM scenario.

experimental measurement of its mass to be 125 GeV and allowing upto  $\pm 2$  GeV error in its model prediction. We set the enlargement factor reduction parameter to 0.3 and the evidence tolerance factor to a rather small value of 0.2, so that while the package sampled more concentratedly near the central mass value, a sufficiently large number of points were collected before the scan converged. In each of the first two sets of scans we required  $H_1$  to be the  $H_{\text{obs}}$ . In the third set we imposed this requirement of consistency with the  $H_{\text{obs}}$  mass on  $H_2$ , in the fourth on  $H_3$ , in the fifth on both  $H_1, H_2$  and in the sixth on both  $H_2, H_3$ . Each of the six sets further contained five separate scans corresponding to  $\phi_\kappa = 0^\circ, 3^\circ, 10^\circ, 30^\circ$  and  $60^\circ$ .

The scanned ranges of the nine free parameters (after fixing the phases) of the natural NMSSM, which are uniform across all its five scenarios considered, are given in tab. 1(a). Only large values of  $\lambda$  and  $\kappa$  are used in this model (with the upper cut-off on them imposed to avoid the Landau pole). Since large radiative corrections from SUSY sectors are not necessary in the natural limit of the NMSSM, the parameters  $M_0, M_{1/2}$  and  $A_0$  are not required to take too large values. Note that while  $A_0$  can in principle be both positive and negative, with a slightly different impact on the physical mass of the SM-like Higgs boson for an identical set of other input parameters in each case, we restricted the scans to its negative values only, in order to increase the scanning efficiency.

In the remaining sixth scan, we considered the complementary parameter space of the NMSSM, with  $\lambda$  and  $\kappa$  kept to relatively smaller (and  $\tan \beta$  to larger) values, so as to prevent too large a singlet-doublet mixing. In fact, for  $\lambda, \kappa \rightarrow 0$ , when the singlet sector gets effectively decoupled,  $H_1$ , which is by default identified with the  $H_{\text{obs}}$ , has properties very identical to the lightest Higgs boson of the MSSM. Since  $H_1$  in such a case does not obtain a maximal tree-level mass that is possible in the most general model, large radiative corrections are needed from the SUSY sector. Hence we used slightly extended ranges of the remaining parameters, which are given in tab. 1(b). This scenario, which we refer to as the low- $\lambda$ -NMSSM scenario henceforth, has been included in our analysis in order to compare the inferences made for the natural NMSSM with an approximate MSSM limit of the model.

Once the scans had completed, we filtered the points obtained with each by further imposing  $123 \text{ GeV} \leq m_{H_{\text{obs}}} \leq 127 \text{ GeV}$ . Note that in the  $H_{\text{obs}} = H_1 + H_2$  and  $H_{\text{obs}} = H_2 + H_3$  scenarios, this condition was imposed on  $H_2$ , since in both these scenarios it is typically the Higgs boson with SM-like couplings. The total number of points,  $N_{\text{total}}$ , remaining after this filter is given in

Scenario	low- $\lambda$	$H_{\text{obs}} = H_1$	$H_{\text{obs}} = H_2$	$H_{\text{obs}} = H_3$	$H_{\text{obs}} = H_1 + H_2$	$H_{\text{obs}} = H_2 + H_3$
$\phi_\kappa = 0^\circ$						
$N_{\text{total}}$	17786	15675	15072	14431	26045	23736
$N_{\text{HB}}$	17722	13691	2904	965	11878	2819
$\phi_\kappa = 3^\circ$						
$N_{\text{total}}$	17829	15775	15026	14806	27199	25684
$N_{\text{HB}}$	17782	13885	3235	2391	11863	1659
$\phi_\kappa = 10^\circ$						
$N_{\text{total}}$	17847	15784	15080	14810	26735	28348
$N_{\text{HB}}$	17786	13866	2411	2495	12607	3369
$\phi_\kappa = 30^\circ$						
$N_{\text{total}}$	17810	16256	15037	14671	31719	28685
$N_{\text{HB}}$	17743	14725	247	276	13503	2012
$\phi_\kappa = 60^\circ$						
$N_{\text{total}}$	17810	0	14996	14438	0	30412
$N_{\text{HB}}$	17743	0	247	2	0	242

Table 2: Number of scanned points remaining after imposing the mass constraint on  $H_{\text{obs}}$  and those passing the HiggsBounds test, for each scenario studied. See text for details.

tab. 2 for each scenario considered. All these points were then tested for consistency with the LEP and LHC exclusion limits on the other, non-SM-like, Higgs bosons of the model, using the package HiggsBounds v4.2.0 [40]. The points passing the HiggsBounds test were retained as the ‘good points’ for further analysis, and their number, denoted by  $N_{\text{HB}}$ , for each scenario is also given in tab. 2. We point out for later reference that in each of the two  $H_{\text{obs}} = H_1$  scenarios as well as in the  $H_{\text{obs}} = H_1 + H_2$  scenario, the number of surviving good points (where they are available) is very identical across all input values of  $\phi_\kappa$ , implying mutually fairly consistent sample sizes.

Next we carried out fits to the  $H_{\text{obs}}$  data for the good points using the public code HiggsSignals v1.3.2 [35]. For obtaining these fits, HiggsSignals requires, along with the masses and BRs of each Higgs boson,  $H_i$ , the square of its normalised effective couplings,  $(g_{H_i X}/g_{h_{\text{SM}} X})^2$ , to a given SM particle pair  $X$ , with  $h_{\text{SM}}$  being the SM Higgs boson with the same mass as the  $H_i$ . Note that when  $X$  is a pair of fermions, there is a scalar as well as a pseudoscalar normalised coupling for each  $H_i$ , both of which need to be passed separately to HiggsSignals. All these are then used to calculate the normalised cross sections,

$$\mu_{H_i}^X \equiv \frac{\sigma(pp \rightarrow H_i \rightarrow X)}{\sigma(pp \rightarrow h_{\text{SM}} \rightarrow X)}, \quad (10)$$

corresponding to a given decay channel,  $X$ , in an approximate way. The NMSSMCALC version we used did not provide the normalised Higgs boson couplings as an output. We therefore modified the code to obtain these couplings for adding them as a dedicated block in the SLHA input file for HiggsSignals.

The program HiggsSignals compares the computed  $\mu_{H_i}^X$  for each  $H_i$  with the experimentally measured ones,  $\mu_{\text{exp}}^X$ , for wide ranges of input Higgs boson masses in a variety of its production and decay channels at the LHC and the Tevatron. We used only the ‘peak-centred’ method and the ‘latestresults’ observable set in the program, with the assignment range variable  $\Lambda$  set to the default value of 1. It thus performed a fit to a total of 81 Higgs boson peak observables (77 from signal strength and 4 from mass measurements), from the CMS, ATLAS, CDF and DØ collaborations,

for a given model point. We assumed a Gaussian theoretical uncertainty of 2 GeV in the masses of the three lightest neutral Higgs bosons of the model. The default values of the uncertainties in the Higgs boson production cross sections as well as BRs were retained. Further details about the fitting procedure can be found in the manual [35] of the package. The main output of HiggsSignals contains the total  $\chi^2$  and the  $p$ -value from the fit, given the number of statistical degrees of freedom, for each model point. Since the aim of this study is a comparison of various  $H_{\text{obs}}$  scenarios rather than the overall goodness of fit for each, we will quantify our results only in terms of the  $\chi^2$  and ignore the  $p$ -value.

As an observable indication of the presence of more than one Higgs bosons near 125 GeV, the double ratios

$$D_1 = \frac{R_{\text{VBF}}^h(\gamma\gamma)/R_{gg}^h(\gamma\gamma)}{R_{\text{VBF}}^h(bb)/R_{gg}^h(bb)}; \quad D_2 = \frac{R_{\text{VBF}}^h(\gamma\gamma)/R_{gg}^h(\gamma\gamma)}{R_{\text{VBF}}^h(WW)/R_{gg}^h(WW)}; \quad D_3 = \frac{R_{\text{VBF}}^h(WW)/R_{gg}^h(WW)}{R_{\text{VBF}}^h(bb)/R_{gg}^h(bb)}, \quad (11)$$

were proposed in [36]. Each of these ratios should be unity if the  $H_{\text{obs}}$  constitutes of only a single Higgs boson, while the contribution of two (or more) Higgs bosons to the  $H_{\text{obs}}$  signal could result in a deviation of these ratios from 1. In the above expressions,  $R_Y^h(X) = R_Y^{H_i}(X) + R_Y^{H_j}(X)$ , where  $H_i$  and  $H_j$  are the two mass-degenerate Higgs bosons in a given scenario and the subscripts VBF and  $gg$  imply the vector boson fusion and the gluon fusion production modes, respectively.  $R_Y^{H_i}(X)$  for each  $H_i$  is defined as

$$R_Y^{H_i}(X) \equiv \frac{\Gamma(H_i \rightarrow Y)}{\Gamma(h_{\text{SM}} \rightarrow Y)} \times \frac{\text{BR}(H_i \rightarrow X)}{\text{BR}(h_{\text{SM}} \rightarrow X)} = \frac{C_Y^{H_i} C_X^{H_i}}{\Gamma_{H_i}/\Gamma_{h_{\text{SM}}}}, \quad (12)$$

with  $Y$  being the given production mode and, in the last equality,  $C_{X(Y)}^{H_i} = \Gamma(H_i \rightarrow X(Y))/\Gamma(h_{\text{SM}} \rightarrow X(Y))$ , the normalised partial decay width of  $H_i$  into the  $X$  ( $Y$ ) pair.<sup>1</sup>  $\Gamma_{H_i}$  and  $\Gamma_{h_{\text{SM}}}$  are the total decay widths of  $H_i$  and  $h_{\text{SM}}$ , respectively.

We also evaluated the ratios  $D_1$ ,  $D_2$  and  $D_3$  for the points which give reasonably good fits to the data (to be defined later) in the scenarios with two mass-degenerate Higgs bosons. For this purpose,  $R_Y^{H_i}(X)$  for each  $H_i$  was calculated by fixing  $\Gamma_{h_{\text{SM}}}$  in eq. (12) to  $4.105 \times 10^{-3}$  GeV, which is the value given by the program HDECAY [41] for a 125 GeV  $h_{\text{SM}}$ . A change of  $\pm 2$  GeV in the mass of  $h_{\text{SM}}$  has only a marginal affect on this width, which we ignore. For calculating the  $\Gamma_{h_{\text{SM}}}$  with HDECAY, care was taken that all the partial decay widths of  $h_{\text{SM}}$  were evaluated at the same perturbative order as that implemented in NMSSMCALC for computing  $\Gamma_{H_i}$ . Moreover,  $C_Y^{H_i}$  is simply the squared normalised coupling of  $H_i$  to a vector boson,  $V$ , pair for the VBF production mode and to a gluon pair for the  $gg$  mode. Similarly,  $C_X^{H_i}$  implies the  $H_i VV$  and  $H_i \gamma\gamma$  normalised couplings squared, respectively, for  $X = WW$  and  $\gamma\gamma$ . All these couplings are thus the same ones obtained from NMSSMCALC for passing to HiggsSignals. In the case of  $X = b\bar{b}$ , though, there is a scalar and pseudoscalar coupling for each  $H_i$ , as noted above. For this reason,  $C_{b\bar{b}}^{H_i}$ 's were calculated using the actual  $\Gamma(H_i \rightarrow b\bar{b})$  from the NMSSMCALC output for a given model point and the  $\Gamma(h_{\text{SM}} \rightarrow b\bar{b})$  obtained from HDECAY for  $m_{h_{\text{SM}}} = 125$  GeV.

## 4 Results and discussion

In fig. 1 we show the total  $\chi^2$  obtained for the points from our scans for the various  $H_{\text{obs}}$  scenarios considered. The green points in the figure correspond to  $\phi_\kappa = 0^\circ$ , violet to  $\phi_\kappa = 3^\circ$ , blue to

<sup>1</sup>Note that eq. (12) assumes that the  $h_{\text{SM}}$ -normalised production cross sections for the  $Y = \text{VBF}$  and  $gg$  processes can be approximated by the normalised partial decay widths of  $H_i$  in the  $VV$  and  $gg$  decay channels, respectively.

$\phi_\kappa = 10^\circ$ , red to  $\phi_\kappa = 30^\circ$  and cyan to  $\phi_\kappa = 60^\circ$ . For the scenarios in which only one of the three lightest neutral Higgs bosons is assumed to be the  $H_{\text{obs}}$ , we have made sure that the difference between the mass of  $H_{\text{obs}}$  and that of each additional Higgs boson nearest to it is always larger than 2.5 GeV. The lower cut-off in  $\chi^2$  in each panel, in this figure and in those that follow, varies depending on the minimum value obtained in the corresponding scenario. The upper cut-off in  $\chi^2$  for each scenario is chosen so as to include as many points in the corresponding figures as possible without the  $\chi^2$  getting more than 10 units larger than the minimum obtained in that scenario (given that there are 9 statistical degrees of freedom).

Fig. 1(a) corresponds to the low- $\lambda$ -NMSSM scenario. One notices in the figure that for  $\phi_\kappa = 0^\circ$  the  $\chi_{\text{min}}^2$  lies very close to 70, and is thus almost identical to  $\chi_{\text{min}}^2 = 69.96$  that is given by HiggsSignals for a SM Higgs boson at a mass of 125.1 GeV, with the same settings as used by us. The input parameters (with the exception of  $M_0$ ,  $M_{1/2}$  and  $A_0$ , which can be adjusted with much more freedom) and the masses of the three lightest Higgs bosons are given in tab. 3. The negligibly small difference in the  $\chi_{\text{min}}^2$  value obtained for the  $h_{\text{SM}}$  and for the CP-conserving low- $\lambda$ -NMSSM results from the fact that  $\lambda$  for the corresponding point in the latter is non-vanishing, as seen in the table, so that the singlet sector is not completely decoupled and an exact MSSM-limit is not reached. One can notice in the figure and the table a slightly lower value of  $\chi_{\text{min}}^2$  obtained for the sets of points corresponding to non-zero  $\phi_\kappa$  values. However,  $\lambda$  for all these points is even larger than in the CP-conserving limit. Note also that, for all  $\phi_\kappa$ , most of the points give  $\Delta\chi^2 \leq 1$ .

In fig. 1(b), which corresponds to the  $H_{\text{obs}} = H_1$  scenario in the natural NMSSM, we see that there is a large concentration of points above a  $\chi^2$  value which is very similar to the  $\chi_{\text{min}}^2$  seen in the adjacent fig. 1(a), for each corresponding  $\phi_\kappa$ . For non-zero  $\phi_\kappa$  though, one also sees a few scattered points with  $\chi^2$  lower than that for any of the points in the high concentration region. The overall lowest  $\chi^2$  lies very close to 68, for  $\phi_\kappa = 30^\circ$ , with the mass of  $H_{\text{obs}}$  for the corresponding point lying at 124.5 GeV. However, according to tab. 3, the mass of  $H_2$  for this point is within 3 GeV of that of  $H_1$ . It is therefore very likely that the relatively better fit for this particular point is a result of the assignment of  $H_2$  instead of or along with  $H_1$  to some of the observables, especially when their experimental mass resolution is relatively poor. This possibility, which implies that our assumption of two Higgs bosons being individually irresolvable if their masses lie within 2.5 GeV of each other is rather robust, will be discussed further later. For  $\phi_\kappa = 60^\circ$  none of the points obtained in the scan for this scenario had  $H_1$  heavier than 123 GeV.

In the  $H_{\text{obs}} = H_2$  scenario, a much smaller number of points was passed by HiggsBounds compared to the  $H_{\text{obs}} = H_1$  scenario, as seen in Fig. 1(c), but the  $\chi_{\text{min}}^2$  is equally low for most  $\phi_\kappa$  here, including  $0^\circ$ . Only for  $\phi_\kappa = 60^\circ$ , while plenty of points with  $m_{H_2} \approx 125$  GeV were obtained in the scan, the  $\chi^2$  for them is never low enough to appear in the figure. Once again, in tab. 3 one can see that, for the points giving the lowest  $\chi^2$  for each  $\phi_\kappa$  in this scenario,  $H_1$  always lies within 3-4 GeV of  $H_2$ . Hence the slightly better fit for this point is again made possible by a contribution of  $H_1$  to some search channels. In fig. 1(d) for the  $H_{\text{obs}} = H_3$  scenario, although very few points with  $\Delta\chi^2 < 10$  appear in this scenario compared to the ones above, the  $\chi_{\text{min}}^2$  is very similar, except for the  $\phi_\kappa = 0^\circ$  case, when it has a fairly high value of around 77.

In fig. 1(e) is shown the total  $\chi^2$  for the  $H_{\text{obs}} = H_1 + H_2$  scenario against the  $H_2$  mass. One can observe quite a few similarities between this figure and the fig. 1(b) seen above (for the  $H_{\text{obs}} = H_1$  scenario). There is once again a large concentration of points with  $\chi^2 \gtrsim 69$  for all  $\phi_\kappa$  except  $60^\circ$ , and also many scattered points below it. Importantly though, there are many points in this scenario which give a  $\chi^2$  lower than 68, which is the overall lowest value observed for any other scenario here. Most of these points, including the one with the overall lowest  $\chi^2$  of  $\sim 65$ , correspond to  $\phi_\kappa = 10^\circ$ , although some points for other  $\phi_\kappa$  can also be noticed. In fig. 1(f) one sees a  $\chi_{\text{min}}^2$  of 68 for the  $H_{\text{obs}} = H_2 + H_3$  scenario also but very few points with  $\chi^2 < 71$ , in contrast with the

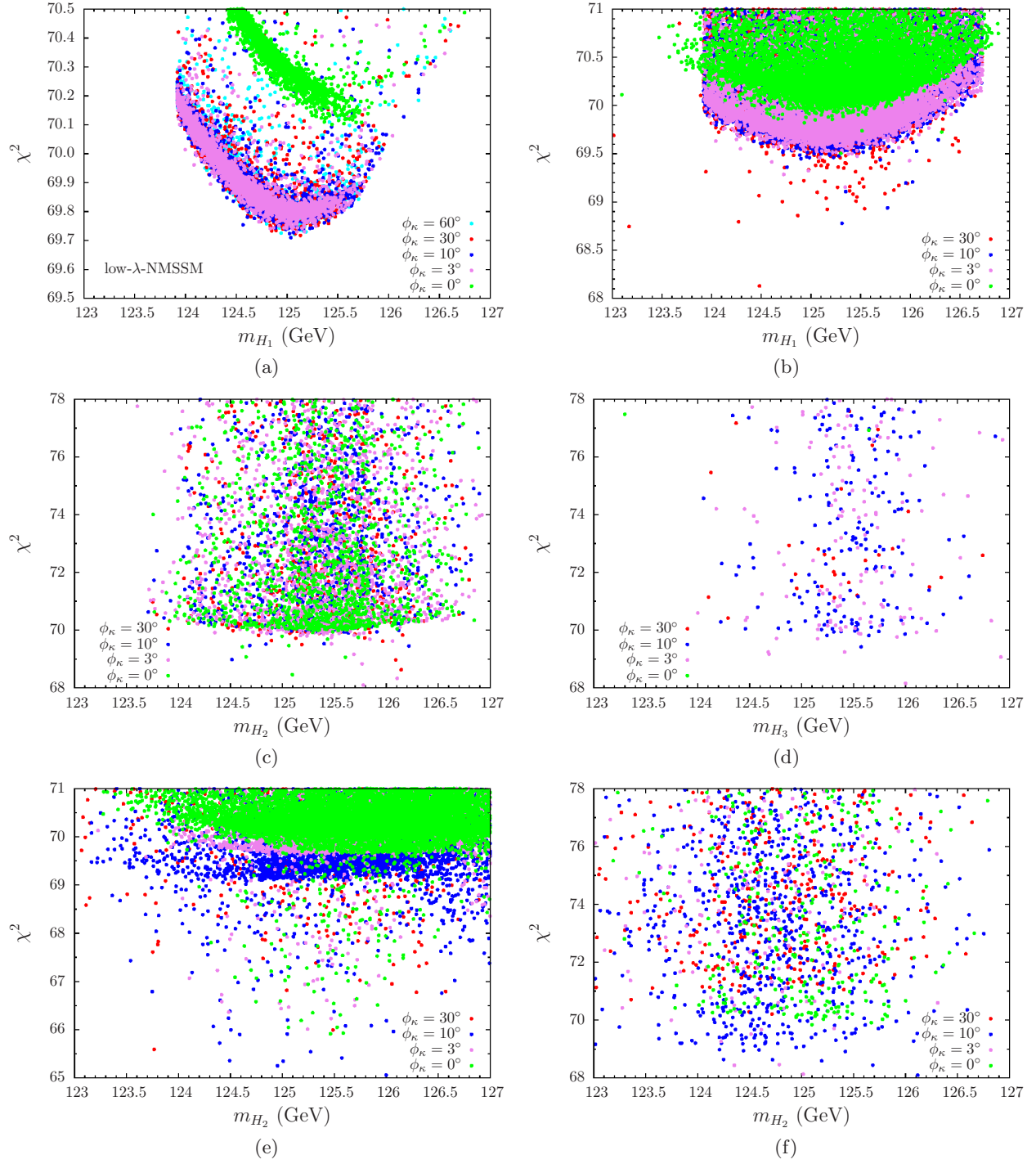


Figure 1: Total  $\chi^2$  as a function of: (a, b)  $m_{H_1}$  when only  $H_1$  is assumed to be the  $H_{\text{obs}}$ , for two different sets of scanned ranges of the parameter space (see text for details); (c)  $m_{H_2}$  when only  $H_2$  is the  $H_{\text{obs}}$ ; (d)  $m_{H_3}$  when only  $H_3$  is the  $H_{\text{obs}}$ ; (e)  $m_{H_2}$  when both  $H_1$  and  $H_2$  lie near 125 GeV and (f)  $m_{H_2}$  when both  $H_2$  and  $H_3$  lie near 125 GeV.

Scenario	low- $\lambda$	$H_{\text{obs}} = H_1$	$H_{\text{obs}} = H_2$	$H_{\text{obs}} = H_3$	$H_{\text{obs}} = H_1 + H_2$	$H_{\text{obs}} = H_2 + H_3$
$\phi_\kappa = 0^\circ$						
$\chi_{\text{min}}^2$	70.1	69.5	68.5	76.9	65.9	69.8
$\lambda$	0.046	0.582	0.653	0.48	0.597	0.597
$\kappa$	0.213	0.43	0.511	0.305	0.302	0.327
$\tan \beta$	17.65	1.66	3.6	6.98	2.39	2.07
$A_\lambda$	853.6	226.8	609.7	680.7	540.0	179.3
$A_\kappa$	-2352	-741.4	-666.0	14.05	-479.3	-3.95
$\mu_{\text{eff}}$	130.0	281.5	243.7	102.6	285.2	112.3
$m_{H_1}$	125.4	125.3	122.1	66.8	123.3	115.1
$m_{H_2}$	162.8	142.1	125.1	121.0	125.5	125.1
$m_{H_3}$	1828	510.6	618.5	125.7	730.0	126.6
$\phi_\kappa = 3^\circ$						
$\chi_{\text{min}}^2$	69.7	69.2	68.1	68.2	66.0	68.1
$\lambda$	0.184	0.639	0.588	0.662	0.631	0.636
$\kappa$	0.291	0.523	0.39	0.349	0.373	0.318
$\tan \beta$	29.6	1.81	2.61	4.24	1.61	6.45
$A_\lambda$	2175	162.5	459.6	425.6	222.0	848.6
$A_\kappa$	-236.7	-595.1	-597.6	-12.03	345.2	-19.4
$\mu_{\text{eff}}$	177.9	218.8	260.5	110.1	196.4	127.4
$m_{H_1}$	125.1	125.3	122.5	97.2	123.4	105.1
$m_{H_2}$	444.9	141.7	125.8	122.3	125.2	125.0
$m_{H_3}$	496.1	405.5	563.6	126.0	366.3	127.2
$\phi_\kappa = 10^\circ$						
$\chi_{\text{min}}^2$	69.7	68.8	69.0	69.4	65.1	68.1
$\lambda$	0.138	0.68	0.56	0.692	0.688	0.585
$\kappa$	0.219	0.409	0.345	0.338	0.361	0.306
$\tan \beta$	16.7	1.85	1.91	4.88	1.98	7.55
$A_\lambda$	1379	291.6	347.8	557.0	390.8	972.6
$A_\kappa$	-623.8	-476.1	-567.8	12.7	-435.1	-30.62
$\mu_{\text{eff}}$	133.5	251.0	266.9	124.3	254.0	136.7
$m_{H_1}$	125.0	125.3	120.3	106.4	123.6	118.7
$m_{H_2}$	212.2	140.5	124.5	111.6	126.0	126.1
$m_{H_3}$	631.6	482.5	541.8	125.6	440.1	127.4
$\phi_\kappa = 30^\circ$						
$\chi_{\text{min}}^2$	69.7	68.1	68.6	70.4	65.6	70.2
$\lambda$	0.136	0.648	0.679	0.537	0.624	0.481
$\kappa$	0.219	0.319	0.586	0.303	0.388	0.311
$\tan \beta$	29.4	2.2	2.13	6.55	2.10	7.67
$A_\lambda$	3515	570.1	295.0	702.2	345.7	796.5
$A_\kappa$	-781.0	-398.4	-590.7	7.07	330.5	-23.22
$\mu_{\text{eff}}$	170.8	288.5	227.8	112.6	209.1	110.0
$m_{H_1}$	125.1	124.5	123.1	86.5	121.6	107.1
$m_{H_2}$	234.3	127.4	126.1	116.8	123.8	124.7
$m_{H_3}$	857.7	462.4	507.8	124.3	405.8	125.8

Table 3: Input parameters and Higgs boson masses corresponding to the points giving the lowest  $\chi^2$  for all  $\phi_\kappa$  cases in each of the  $H_{\text{obs}}$  scenarios considered.

$H_{\text{obs}} = H_1$  and  $H_{\text{obs}} = H_1 + H_2$  scenarios but similarly to the  $H_{\text{obs}} = H_2$  and  $H_{\text{obs}} = H_3$  scenarios.

From the above discussion, it is clear that certain points, or parameter space configurations, in the  $H_{\text{obs}} = H_1 + H_2$  scenario give the best fit to the current experimental Higgs boson data. A *global*  $\chi^2_{\text{min}}$ , i.e., the lowest  $\chi^2$  value across all scenarios examined here, of around 65 has been observed for  $\phi_\kappa = 10^\circ$  in this scenario, with some points corresponding to other values of  $\phi_\kappa$  also lying within 1 unit of this  $\chi^2$ . None of the points obtained for the other scenarios gives a  $\chi^2$  lying even within 3 units of this global minimum, despite the number of sampled points for the  $H_{\text{obs}} = H_1$  scenario being typically larger. The reason for a better fit for some points with two nearly degenerate Higgs bosons becomes apparent by looking at the detailed output of HiggsSignals. In the peak-centred method, HiggsSignals assigns to a given observable the Higgs boson with a mass closest to the measured mass provided by the experiment. This mass measurement currently ranges between 124.7 GeV to 126.0 GeV. Thus, when a single Higgs boson is assigned to all the observables, the  $\chi^2$  contribution is large from the observables for which the measured mass lies away from the mass of the assigned Higgs boson, and the experimental mass resolution is good. On the other hand, when two Higgs bosons lie close to each other, the one assigned to a given observable is the one for which the difference of the predicted mass from the experimental value is the smallest, so that the  $\chi^2$  contribution from this observable is minimal. This is as long as the mass of the other Higgs boson nearby lies outside the experimental mass resolution, otherwise HiggsSignals automatically assigns both the Higgs bosons to an individual observable if it improves the fit.

Some caveats are in order here though. A  $\Delta\chi^2 \simeq 3$  is statistically quite insignificant for drawing any concrete inferences about the considered scenarios, since the total number of observables and statistical degrees of freedom is quite large. At the same time, the number of points giving  $\Delta\chi^2 \leq 3$  is also fairly small. Moreover, no other experimental constraints have been imposed in our analysis, since the publicly available tools for testing these are so far not compatible with the cNMSSM. It is thus possible that many of the interesting points may have already been ruled out by such constraints. However, the aim of this study is not to disregard one scenario in favour of another, but to simply show that, given the current experimental data, the scenario with two mass-degenerate Higgs bosons in the NMSSM provides as good, if not better, a fit as the scenarios with a single Higgs boson near 125 GeV. This alternative possibility even points towards a source of CP-violation beyond the SM and, therefore, warrants more dedicated analyses as well experimental probes. In the following we discuss some other interesting aspects of this scenario.

In the left, middle and right panels of fig. 2 we show the ratios  $D_1$ ,  $D_2$  and  $D_3$ , respectively, as functions of the mass difference,  $m_{H_2} - m_{H_1}$ , for various  $\phi_\kappa$  values in the  $H_{\text{obs}} = H_1 + H_2$  scenario. The heat map corresponds to the total  $\chi^2$  obtained for the points shown in each panel. This  $\chi^2$  has a uniform upper cut-off of 71 across all panels, as in fig. 1(e), but its lower cut-off varies according to the minimum obtained for the  $\phi_\kappa$  case that a given panel corresponds to. According to fig. 2(a), for  $\phi_\kappa = 0^\circ$  the three ratios remain largely close to unity, but deviations up to 15–20% can be seen for some points.  $D_2$ , the ratio dependent on only the bosonic signal strengths, only gets smaller than 1 for some points and its maximum observed deviation is lower than that of  $D_1$  and  $D_3$ , each of which can be both above or below unity. Importantly, the points for which a large deviation of each ratio from 1 is seen are also generally the ones giving a relatively good  $\chi^2$  fit to the data.

A similar trend is seen also for other values of  $\phi_\kappa$ . However, deviations of  $D_1$  and  $D_2$  from unity by up to 40–50% are obtained for  $\phi_\kappa = 3^\circ$  (fig. 2(b)) and  $\phi_\kappa = 10^\circ$  (fig. 2(c)), but there are many more points with significantly large deviations of each of the ratios for the latter phase compared to the former one. For  $\phi_\kappa = 30^\circ$  all the points appearing in fig. 2(d) give  $D_1$ ,  $D_2$  and  $D_3$  smaller than 1 and the overall deviation is generally smaller than for other non-zero phases but larger than for the rNMSSM limit. Thus, for this phase, the measured signal strengths can provide a clear indication whenever two Higgs bosons are present near 125 GeV instead of one. The reason

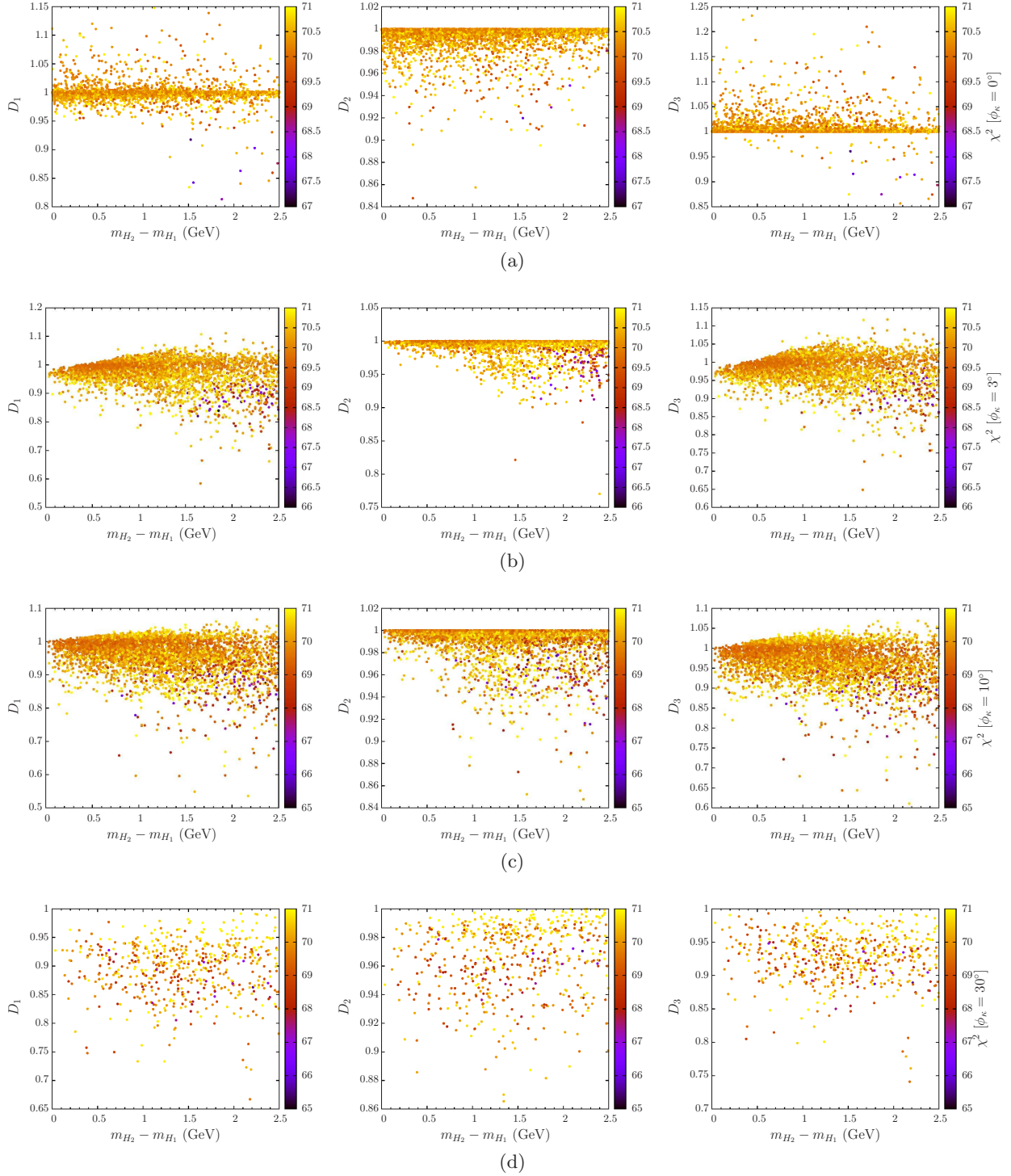


Figure 2: The ratios  $D_1$ ,  $D_2$  and  $D_3$ , defined in eq. (11), as functions of the difference between  $H_2$  and  $H_1$  masses, in the scenario when  $H_{\text{obs}} = H_1 + H_2$ . In (a)  $\phi_\kappa$  is set to  $0^\circ$ , in (b) to  $3^\circ$ , in (c) to  $10^\circ$  and in (d) to  $30^\circ$ . The heat map in all the panels corresponds to the total  $\chi^2$ .

why the deviations of the three ratios are much smaller overall in the case of  $\phi_\kappa = 0^\circ$  than for the CPV cases, for points showing the highest consistency with the data, will become clearer below.

As noted earlier, a scenario with two mass-degenerate Higgs bosons in the cNMSSM entails both the  $H_{\text{obs}} = H_1 + H_2$  and  $H_{\text{obs}} = H_1/H_2 + A_1$  possibilities of the rNMSSM. Thus it is interesting to see which one of these two possibilities is favoured more by the data, for a given  $\phi_\kappa$ . In the left panels of fig. 3 we thus show the squared normalised coupling  $C_{VV}^{H_2}$  against  $C_{VV}^{H_1}$ , with the heat map corresponding to the total  $\chi^2$ . Similarly, in the right panels we have plotted  $C_{VV}^{H_3}$  vs.  $C_{VV}^{H_1}$ , while the distribution of  $m_{H_3}$  is shown by the heat map. For clarity of observation, we have included in this figure points with a total  $\chi^2$  reaching up to 80, which is much higher than for the points shown in the earlier figures for this scenario. Also we have imposed an upper cut-off of 300 GeV on the mass of  $H_3$ . We expect  $C_{VV}^{H_i}$  to either vanish when a given  $H_i$  is a pure pseudoscalar (in the rNMSSM limit) or be relatively small when it is pseudoscalar-like (for  $\phi_\kappa > 0^\circ$ ). Note that these couplings satisfy the sum rule [26]

$$\sum_{i=1}^N C_{VV}^{H_i} \simeq 1, \quad (13)$$

where  $N$  is the total number of neutral Higgs bosons that have a tree-level coupling to the gauge bosons, i.e., 5 in the cNMSSM and 3 in the rNMSSM limit.<sup>2</sup> In the figure we see the above sum rule being satisfied almost completely by the three lightest neutral Higgs bosons under consideration here, implying that the remaining two doublet-like Higgs bosons are nearly decoupled.

In the case of  $\phi_\kappa = 0^\circ$  (i.e., in the rNMSSM limit) in the left panel of fig. 3(a), we see two distinct kinds of points. There are some points lying along the diagonal, for which  $C_{VV}^{H_1}$  and  $C_{VV}^{H_2}$  alone are enough to satisfy the sum rule in eq. (13). It is further evident from the right panel that  $C_{VV}^{H_3}$  for these points is exactly 0.  $H_1$  and  $H_2$  in these points should thus be scalars and  $H_3$  a pseudoscalar (i.e.,  $A_1$ ). But for the majority of the points, which lies along either of the axes,  $C_{VV}^{H_1}$  is nearly 1, implying it is an almost pure doublet-like scalar, while  $C_{VV}^{H_2}$  is exactly 0, implying it is a pseudoscalar, or vice versa. One can then observe in the right panel that for such points  $C_{VV}^{H_3}$ , with  $H_3$  being the singlet-like scalar, is responsible for the sum rule being satisfied. Thus when the doublet-like scalar, whether  $H_1$  or  $H_2$ , has  $C_{VV}^{H_i}$  slightly below 1,  $C_{VV}^{H_3}$  is slightly above 0. The mixing of the doublet scalar with  $H_3$  increases as its mass decreases, as is evident from the heat map in the right panel of the figure. As a result, the largest  $C_{VV}^{H_3}$ ,  $\sim 0.8$ , is seen for the lowest  $m_{H_3}$  obtained, which lies just above the allowed  $H_{\text{obs}}$  mass window.

A closer inspection of the heat map in the left panel of fig. 3(a) reveals that the lowest values of  $\chi^2$  are obtained for points lying along one of the axes, i.e., when the doublet-like scalar is nearly mass degenerate with the pseudoscalar. For points along the diagonal, the  $\chi^2$  is in fact always larger than 71. This is the reason for the relatively small deviations of  $D_1$ ,  $D_2$  and  $D_3$  from 1 seen in fig. 2(a), where only points with  $\chi^2$  lower than 71 were shown. For such points, since one of the  $H_1$  and  $H_2$  is a pure pseudoscalar as well as singlet-dominated, its contribution to the combined signal strength in the  $WW$  channel is null and that in the  $\gamma\gamma$  and  $b\bar{b}$  channels is minimal. Therefore, while the presence of  $H_1$  and  $H_2$  of the rNMSSM near 125 GeV may possibly cause  $D_1$ ,  $D_2$  and  $D_3$  to deviate more significantly from 1, the consistency of this scenario with the LHC data is worse than that of the  $H_1 + A_1$  scenario.

Fig. 3(b) shows that, for  $\phi_\kappa = 3^\circ$ ,  $H_1$  and  $H_2$  are almost always scalar-like while  $H_3$  is highly pseudoscalar-like with a relatively much smaller  $C_{VV}^{H_3}$  generally. However, due to CP-mixing,  $C_{VV}^{H_3}$

---

<sup>2</sup>Note that since the  $h_{\text{SM}}$  is a hypothetical SM Higgs boson with the same mass as a given  $H_i$ , at the tree level the ratio  $C_X^{H_i}$  in fact corresponds to  $(g_{H_i X}/g_{h_{\text{SM}} X})^2$  and the equality in eq. (13) is exact. However, since  $C_X^{H_i}$  have actually been defined here in terms of the partial decay widths of  $H_i$  in the  $X$  channel, which include higher order effects also, the sum of  $C_X^{H_i}$  may deviate slightly from unity.

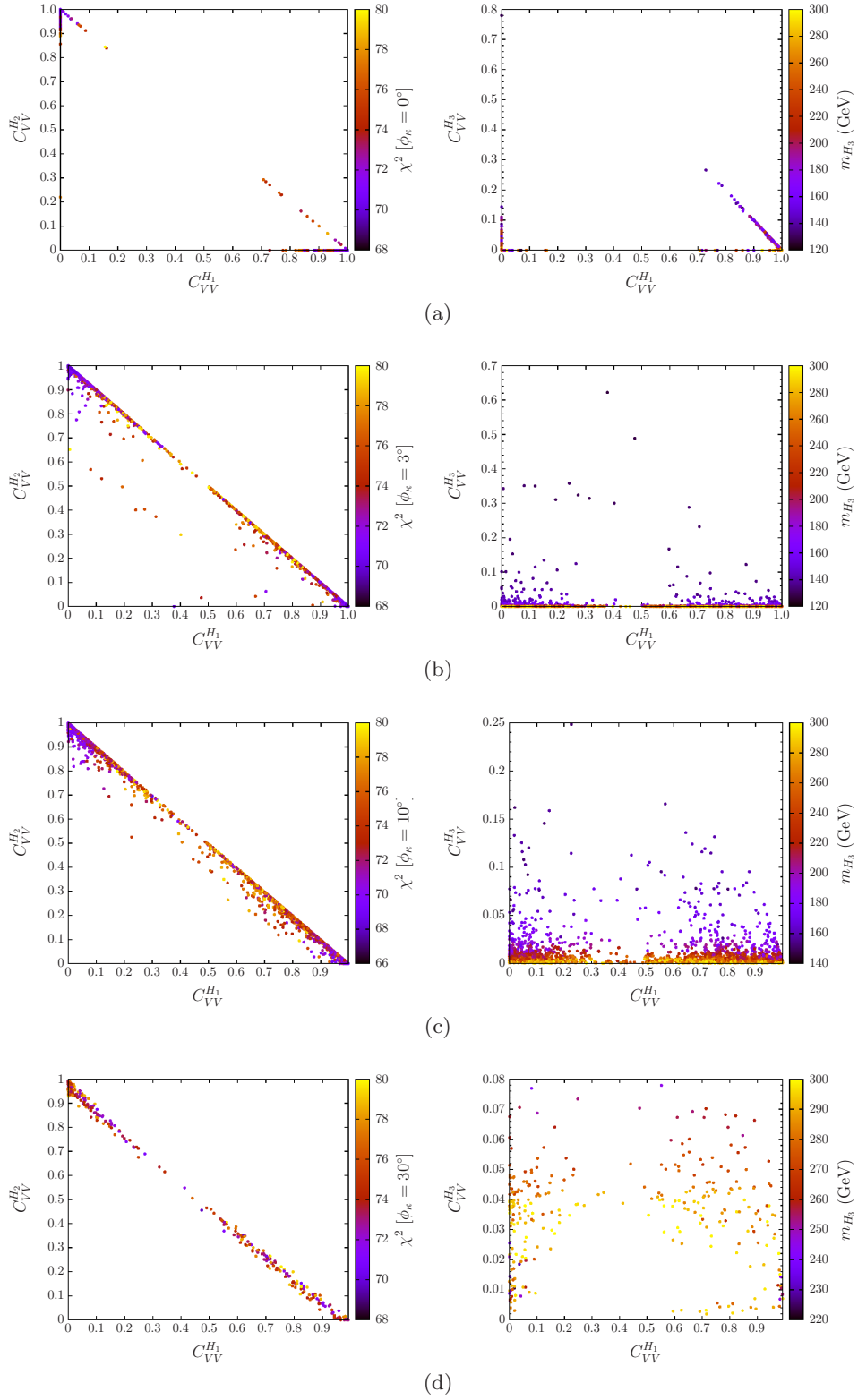


Figure 3: Squared normalised coupling of  $H_1$  to the gauge bosons vs. that of  $H_2$  (left) and of  $H_3$  (right) in the scenario when  $H_{\text{obs}} = H_1 + H_2$ , with  $\phi_\kappa$  set to (a)  $0^\circ$ , (b)  $3^\circ$ , (c)  $10^\circ$  and (d)  $30^\circ$ . The heat map in the left panels shows the distribution of  $\chi^2$  and in the right panels that of  $m_{H_3}$ .

can reach as high as 0.7 or so when the mass of  $H_3$  is close to that of  $H_1$  and  $H_2$ , though this happens for only a few points. A very crucial point to note here is that the total  $\chi^2$  in the left panel never falls below 68, which is due to the cut-off on the allowed upper value of  $m_{H_3}$ . This means that the points which give the overall best fit to the data have a much higher  $H_3$  mass, which leads to a much smaller scalar-pseudoscalar mixing and hence negligible  $C_{VV}^{H_3}$ .

For the  $\phi_\kappa = 10^\circ$  case, illustrated in fig. 3(c), while the maximum  $C_{VV}^{H_3}$  obtained is relatively small and hence  $C_{VV}^{H_1}$  and  $C_{VV}^{H_2}$  do not deviate from the diagonal by much in the left panel, there are many more points, compared to the  $\phi_\kappa = 3^\circ$  case above, for which  $C_{VV}^{H_3}$  is significant, according to the right panel. Finally, for  $\phi_\kappa = 30^\circ$ , although  $C_{VV}^{H_3}$  never completely vanishes, it also stays smaller overall than it is for other phases. The reason for this is that the pseudoscalar-like  $H_3$  never achieves a mass below 220 GeV or so, as can be noted from the heat map in the right panel of fig. 3(d). In the left panel one therefore sees that  $C_{VV}^{H_1}$  and  $C_{VV}^{H_2}$  always remain very close to the diagonal. Hence, for non-zero  $\phi_\kappa$  the data clearly favours two scalar-like Higgs bosons near 125 GeV, instead of a pair of scalar-like and pseudoscalar-like Higgs bosons.

## 5 Conclusions

In summary, we have tested the consistency of the real and complex NMSSM with the latest Higgs boson data from the LHC Run-I and the Tevatron. In particular, we have focused on scenarios wherein the resonant peak seen by the experiments can be explained in terms of two nearly mass-degenerate Higgs states around 125 GeV. Such scenarios have been verified in the rNMSSM previously and have not been ruled out yet. What we have shown here is that the possibility of such dynamics being available in the NMSSM is somewhat enhanced if some degree of (explicit) CP-violation is allowed in the Higgs sector. This can be done by assuming one or more of the Higgs sector parameters to be complex. By choosing this parameter to be  $\kappa$ , one can evade the fermion EDM measurements, which tightly constrain the other possibly complex parameters in the Higgs and soft SUSY sectors of the NMSSM.

In order to achieve the above we have performed detailed numerical scans of the parameter space of the cNMSSM to obtain various possible configurations with  $\sim 125$  GeV Higgs boson(s) that also give SM-like signal strengths. In these scans we set the phase of  $\kappa$  to five different values,  $0^\circ$ ,  $3^\circ$ ,  $10^\circ$ ,  $30^\circ$  and  $60^\circ$ . Through a comprehensive analysis of the points obtained from these scans, we have then established that certain parameter configurations yielding two Higgs bosons near 125 GeV are slightly more favoured by the current data compared to scenarios with a single  $\sim 125$  GeV Higgs boson. This statement is even stronger when the two Higgs bosons are CP-mixed states. For the case of  $\phi_\kappa = 10^\circ$  we thus obtained: i) the point with the global minimum  $\chi^2$ ; ii) more points with  $\Delta\chi^2$  lying within 4 units of the global minimum  $\chi^2$  compared to all other scenarios and phases tested; iii) more points with larger deviations of the ratios  $D_1$ ,  $D_2$  and  $D_3$  from unity.

While analysing the aforementioned scenario with two Higgs bosons near 125 GeV, we have made sure that their masses are close enough that these two states cannot be distinguished experimentally as separate particles. In doing so we have exploited the fact that the experimental measurements are currently unable to reconstruct Breit-Wigner resonances, given that the experimental resolution in all channels investigated in the Higgs analyses is significantly larger than the intrinsic Higgs boson widths involved (so that LHC data actually reproduce Gaussian shapes). However, (tree-level) interference and (1-loop) mixing effects become crucial and need to be accounted for when the (pole) mass difference between two Higgs states is comparable or smaller than their individual intrinsic width. While we have ignored such effects here for points where they can be relevant,

which however make up a very tiny fraction of all the good points from our scans, they are the subject of a dedicated separate study [42].

Finally, in our analysis we have used up-to-date sophisticated computational tools in which state-of-the-art theoretical calculations and/or experimental measurements have been implemented, so that the solidity of our results is assured.

## Acknowledgments

S. Munir is thankful to Margarete Mühlleitner for useful discussions regarding the cNMSSM and for help with the NMSSMCALC program. S. Moretti is supported in part through the NExT Institute. S. Munir is supported by the Korea Ministry of Science, ICT and Future Planning, Gyeongsangbuk-Do and Pohang City for Independent Junior Research Groups at the Asia Pacific Center for Theoretical Physics.

## References

- [1] P. Fayet, “Supergauge Invariant Extension of the Higgs Mechanism and a Model for the electron and Its Neutrino,” *Nucl.Phys.* **B90** (1975) 104–124; J. R. Ellis, J. Gunion, H. E. Haber, L. Roszkowski, and F. Zwirner, “Higgs Bosons in a Nonminimal Supersymmetric Model,” *Phys.Rev.* **D39** (1989) 844; L. Durand and J. L. Lopez, “Upper Bounds on Higgs and Top Quark Masses in the Flipped SU(5) x U(1) Superstring Model,” *Phys.Lett.* **B217** (1989) 463; M. Drees, “Supersymmetric Models with Extended Higgs Sector,” *Int.J.Mod.Phys.* **A4** (1989) 3635.
- [2] U. Ellwanger, C. Hugonie, and A. M. Teixeira, “The Next-to-Minimal Supersymmetric Standard Model,” *Phys.Rept.* **496** (2010) 1–77, [arXiv:0910.1785 \[hep-ph\]](#).
- [3] M. Maniatis, “The Next-to-Minimal Supersymmetric extension of the Standard Model reviewed,” *Int.J.Mod.Phys.* **A25** (2010) 3505–3602, [arXiv:0906.0777 \[hep-ph\]](#).
- [4] ATLAS Collaboration, G. Aad *et al.*, “Observation of a new particle in the search for the Standard Model Higgs boson with the ATLAS detector at the LHC,” *Phys.Lett.* **B716** (2012) 1–29, [arXiv:1207.7214 \[hep-ex\]](#).
- [5] CMS Collaboration, S. Chatrchyan *et al.*, “Observation of a new boson at a mass of 125 GeV with the CMS experiment at the LHC,” *Phys.Lett.* **B716** (2012) 30–61, [arXiv:1207.7235 \[hep-ex\]](#).
- [6] CMS Collaboration, S. Chatrchyan *et al.*, “Observation of a new boson with mass near 125 GeV in pp collisions at  $\sqrt{s} = 7$  and 8 TeV,” *JHEP* **1306** (2013) 081, [arXiv:1303.4571 \[hep-ex\]](#).
- [7] U. Ellwanger, “A Higgs boson near 125 GeV with enhanced di-photon signal in the NMSSM,” *JHEP* **1203** (2012) 044, [arXiv:1112.3548 \[hep-ph\]](#); S. King, M. Muhlleitner, and R. Nevzorov, “NMSSM Higgs Benchmarks Near 125 GeV,” *Nucl.Phys.* **B860** (2012) 207–244, [arXiv:1201.2671 \[hep-ph\]](#); J. Cao *et al.*, “A SM-like Higgs near 125 GeV in low energy SUSY: a comparative study for MSSM and NMSSM,” *JHEP* **1203** (2012) 086, [arXiv:1202.5821 \[hep-ph\]](#).
- [8] J. F. Gunion, Y. Jiang, and S. Kraml, “Could two NMSSM Higgs bosons be present near 125 GeV?,” *Phys.Rev.* **D86** (2012) 071702, [arXiv:1207.1545 \[hep-ph\]](#).

- [9] S. King, M. Muhlleitner, R. Nevzorov, and K. Walz, “Natural NMSSM Higgs Bosons,” *Nucl.Phys.* **B870** (2013) 323–352, [arXiv:1211.5074 \[hep-ph\]](#); T. Gherghetta, B. von Harling, A. D. Medina, and M. A. Schmidt, “The Scale-Invariant NMSSM and the 126 GeV Higgs Boson,” *JHEP* **1302** (2013) 032, [arXiv:1212.5243 \[hep-ph\]](#); L. Wu, J. M. Yang, C.-P. Yuan, and M. Zhang, “Higgs self-coupling in the MSSM and NMSSM after the LHC Run 1,” *Phys. Lett.* **B747** (2015) 378–389, [arXiv:1504.06932 \[hep-ph\]](#).
- [10] S. Munir, L. Roszkowski, and S. Trojanowski, “Simultaneous enhancement in  $\gamma\gamma$ ,  $b\bar{b}$  and  $\tau^+\tau^-$  rates in the NMSSM with nearly degenerate scalar and pseudoscalar Higgs bosons,” *Phys. Rev.* **D88** (2013) 055017, [arXiv:1305.0591 \[hep-ph\]](#).
- [11] A. G. Cohen, D. Kaplan, and A. Nelson, “Progress in electroweak baryogenesis,” *Ann.Rev.Nucl.Part.Sci.* **43** (1993) 27–70, [arXiv:hep-ph/9302210 \[hep-ph\]](#); M. Quiros, “Field theory at finite temperature and phase transitions,” *Helv.Phys.Acta* **67** (1994) 451–583.
- [12] A. Sakharov, “Violation of CP Invariance, c Asymmetry, and Baryon Asymmetry of the Universe,” *Pisma Zh.Eksp.Teor.Fiz.* **5** (1967) 32–35.
- [13] T. Ibrahim and P. Nath, “CP Violation From Standard Model to Strings,” *Rev.Mod.Phys.* **80** (2008) 577–631, [arXiv:0705.2008 \[hep-ph\]](#).
- [14] T. Cohen, D. E. Morrissey, and A. Pierce, “Electroweak Baryogenesis and Higgs Signatures,” *Phys.Rev.* **D86** (2012) 013009, [arXiv:1203.2924 \[hep-ph\]](#); D. Curtin, P. Jaiswal, and P. Meade, “Excluding Electroweak Baryogenesis in the MSSM,” *JHEP* **1208** (2012) 005, [arXiv:1203.2932 \[hep-ph\]](#); M. Carena, G. Nardini, M. Quiros, and C. E. Wagner, “MSSM Electroweak Baryogenesis and LHC Data,” *JHEP* **1302** (2013) 001, [arXiv:1207.6330 \[hep-ph\]](#).
- [15] A. Pilaftsis, “CP odd tadpole renormalization of Higgs scalar - pseudoscalar mixing,” *Phys.Rev.* **D58** (1998) 096010, [arXiv:hep-ph/9803297 \[hep-ph\]](#); A. Pilaftsis, “Higgs scalar - pseudoscalar mixing in the minimal supersymmetric standard model,” *Phys.Lett.* **B435** (1998) 88–100, [arXiv:hep-ph/9805373 \[hep-ph\]](#).
- [16] A. Pilaftsis and C. E. Wagner, “Higgs bosons in the minimal supersymmetric standard model with explicit CP violation,” *Nucl.Phys.* **B553** (1999) 3–42, [arXiv:hep-ph/9902371 \[hep-ph\]](#); M. S. Carena, J. R. Ellis, A. Pilaftsis, and C. Wagner, “Renormalization group improved effective potential for the MSSM Higgs sector with explicit CP violation,” *Nucl.Phys.* **B586** (2000) 92–140, [arXiv:hep-ph/0003180 \[hep-ph\]](#).
- [17] S. Choi, M. Drees, and J. S. Lee, “Loop corrections to the neutral Higgs boson sector of the MSSM with explicit CP violation,” *Phys.Lett.* **B481** (2000) 57–66, [arXiv:hep-ph/0002287 \[hep-ph\]](#); M. S. Carena, J. R. Ellis, A. Pilaftsis, and C. Wagner, “Higgs boson pole masses in the MSSM with explicit CP violation,” *Nucl.Phys.* **B625** (2002) 345–371, [arXiv:hep-ph/0111245 \[hep-ph\]](#); M. S. Carena, J. R. Ellis, S. Mrenna, A. Pilaftsis, and C. Wagner, “Collider probes of the MSSM Higgs sector with explicit CP violation,” *Nucl.Phys.* **B659** (2003) 145–178, [arXiv:hep-ph/0211467 \[hep-ph\]](#); S. Choi, J. Kalinowski, Y. Liao, and P. Zerwas, “H/A Higgs mixing in CP-noninvariant supersymmetric theories,” *Eur.Phys.J.* **C40** (2005) 555–564, [arXiv:hep-ph/0407347 \[hep-ph\]](#).

- [18] C. Baker, D. Doyle, P. Geltenbort, K. Green, M. van der Grinten, *et al.*, “An Improved experimental limit on the electric dipole moment of the neutron,” *Phys.Rev.Lett.* **97** (2006) 131801, [arXiv:hep-ex/0602020 \[hep-ex\]](#); E. D. Commins, “Electric dipole moments of elementary particles, nuclei, atoms, and molecules,” *J.Phys.Soc.Jap.* **76** (2007) 111010; W. Griffith, M. Swallows, T. Loftus, M. Romalis, B. Heckel, *et al.*, “Improved Limit on the Permanent Electric Dipole Moment of Hg-199,” *Phys.Rev.Lett.* **102** (2009) 101601.
- [19] S. Abel, S. Khalil, and O. Lebedev, “EDM constraints in supersymmetric theories,” *Nucl.Phys.* **B606** (2001) 151–182, [arXiv:hep-ph/0103320 \[hep-ph\]](#).
- [20] N. Haba, “Explicit CP violation in the Higgs sector of the next-to-minimal supersymmetric standard model,” *Prog.Theor.Phys.* **97** (1997) 301–310, [arXiv:hep-ph/9608357 \[hep-ph\]](#); T. Ibrahim and P. Nath, “The Neutron and the lepton EDMs in MSSM, large CP violating phases, and the cancellation mechanism,” *Phys.Rev.* **D58** (1998) 111301, [arXiv:hep-ph/9807501 \[hep-ph\]](#); M. Boz, “The Higgs sector and electron electric dipole moment in next-to-minimal supersymmetry with explicit CP violation,” *Mod.Phys.Lett.* **A21** (2006) 243–264, [arXiv:hep-ph/0511072 \[hep-ph\]](#); J. R. Ellis, J. S. Lee, and A. Pilaftsis, “Electric Dipole Moments in the MSSM Reloaded,” *JHEP* **0810** (2008) 049, [arXiv:0808.1819 \[hep-ph\]](#); Y. Li, S. Profumo, and M. Ramsey-Musolf, “A Comprehensive Analysis of Electric Dipole Moment Constraints on CP-violating Phases in the MSSM,” *JHEP* **1008** (2010) 062, [arXiv:1006.1440 \[hep-ph\]](#).
- [21] S. Huber and M. Schmidt, “Electroweak baryogenesis: Concrete in a SUSY model with a gauge singlet,” *Nucl.Phys.* **B606** (2001) 183–230, [arXiv:hep-ph/0003122 \[hep-ph\]](#); S. J. Huber, T. Konstandin, T. Prokopec, and M. G. Schmidt, “Baryogenesis in the MSSM, nMSSM and NMSSM,” *Nucl.Phys.* **A785** (2007) 206–209, [arXiv:hep-ph/0608017 \[hep-ph\]](#); S. Kanemura, E. Senaha, and T. Shindou, “First-order electroweak phase transition powered by additional F-term loop effects in an extended supersymmetric Higgs sector,” *Phys.Lett.* **B706** (2011) 40–45, [arXiv:1109.5226 \[hep-ph\]](#); K. Cheung, T.-J. Hou, J. S. Lee, and E. Senaha, “Singlino-driven Electroweak Baryogenesis in the Next-to-MSSM,” *Phys.Lett.* **B710** (2012) 188–191, [arXiv:1201.3781 \[hep-ph\]](#); W. Huang, Z. Kang, J. Shu, P. Wu, and J. M. Yang, “New insights in the electroweak phase transition in the NMSSM,” *Phys.Rev.* **D91** no. 2, (2015) 025006, [arXiv:1405.1152 \[hep-ph\]](#); X.-J. Bi, L. Bian, W. Huang, J. Shu, and P.-F. Yin, “Interpretation of the Galactic Center excess and electroweak phase transition in the NMSSM,” *Phys. Rev.* **D92** no. 2, (2015) 023507, [arXiv:1503.03749 \[hep-ph\]](#).
- [22] S. Moretti, S. Munir, and P. Poulose, “125 GeV Higgs Boson signal within the complex NMSSM,” *Phys.Rev.* **D89** no. 1, (2014) 015022, [arXiv:1305.0166 \[hep-ph\]](#).
- [23] D. A. Demir, “Effects of the supersymmetric phases on the neutral Higgs sector,” *Phys.Rev.* **D60** (1999) 055006, [arXiv:hep-ph/9901389 \[hep-ph\]](#); A. Dedes and S. Moretti, “Effect of large supersymmetric phases on Higgs production,” *Phys.Rev.Lett.* **84** (2000) 22–25, [arXiv:hep-ph/9908516 \[hep-ph\]](#); A. Dedes and S. Moretti, “Effects of CP violating phases on Higgs boson production at hadron colliders in the minimal supersymmetric standard model,” *Nucl.Phys.* **B576** (2000) 29–55, [arXiv:hep-ph/9909418 \[hep-ph\]](#); G. L. Kane and L.-T. Wang, “Implications of supersymmetry phases for Higgs boson signals and limits,” *Phys.Lett.* **B488** (2000) 383–389, [arXiv:hep-ph/0003198 \[hep-ph\]](#); A. Arhrib, D. K. Ghosh, and O. C. Kong, “Observing CP violating MSSM Higgs bosons at hadron colliders?,” *Phys.Lett.* **B537** (2002) 217–226, [arXiv:hep-ph/0112039 \[hep-ph\]](#); S. Choi,

- K. Hagiwara, and J. S. Lee, “Higgs boson decays in the minimal supersymmetric standard model with radiative Higgs sector CP violation,” *Phys.Rev.* **D64** (2001) 032004, [arXiv:hep-ph/0103294 \[hep-ph\]](#); S. Choi, M. Drees, J. S. Lee, and J. Song, “Supersymmetric Higgs boson decays in the MSSM with explicit CP violation,” *Eur.Phys.J.* **C25** (2002) 307–313, [arXiv:hep-ph/0204200 \[hep-ph\]](#); J. R. Ellis, J. S. Lee, and A. Pilaftsis, “CERN LHC signatures of resonant CP violation in a minimal supersymmetric Higgs sector,” *Phys.Rev.* **D70** (2004) 075010, [arXiv:hep-ph/0404167 \[hep-ph\]](#); S. Hesselbach, S. Moretti, S. Munir, and P. Poulose, “Explicit CP violation in the MSSM through  $gg \rightarrow H \rightarrow \gamma\gamma$ ,” *Phys.Rev.* **D82** (2010) 074004, [arXiv:0903.0747 \[hep-ph\]](#); T. Fritzsche, S. Heinemeyer, H. Rzehak, and C. Schappacher, “Heavy Scalar Top Quark Decays in the Complex MSSM: A Full One-Loop Analysis,” *Phys. Rev.* **D86** (2012) 035014, [arXiv:1111.7289 \[hep-ph\]](#); A. Chakraborty, B. Das, J. L. Diaz-Cruz, D. K. Ghosh, S. Moretti, *et al.*, “125 GeV Higgs signal at the LHC in the CP-violating MSSM,” *Phys.Rev.* **D90** no. 5, (2014) 055005, [arXiv:1301.2745 \[hep-ph\]](#).
- [24] K. Funakubo, S. Tao, and F. Toyoda, “Phase transitions in the NMSSM,” *Prog.Theor.Phys.* **114** (2005) 369–389, [arXiv:hep-ph/0501052 \[hep-ph\]](#).
- [25] S. Ham, S. Oh, and D. Son, “Neutral Higgs sector of the next-to-minimal supersymmetric standard model with explicit CP violation,” *Phys.Rev.* **D65** (2002) 075004, [arXiv:hep-ph/0110052 \[hep-ph\]](#); K. Funakubo and S. Tao, “The Higgs sector in the next-to-MSSM,” *Prog.Theor.Phys.* **113** (2005) 821–842, [arXiv:hep-ph/0409294 \[hep-ph\]](#).
- [26] K. Cheung, T.-J. Hou, J. S. Lee, and E. Senaha, “The Higgs Boson Sector of the Next-to-MSSM with CP Violation,” *Phys.Rev.* **D82** (2010) 075007, [arXiv:1006.1458 \[hep-ph\]](#); K. Cheung, T.-J. Hou, J. S. Lee, and E. Senaha, “Higgs Mediated EDMs in the Next-to-MSSM: An Application to Electroweak Baryogenesis,” *Phys.Rev.* **D84** (2011) 015002, [arXiv:1102.5679 \[hep-ph\]](#).
- [27] S. Munir, “Novel Higgs-to-125 GeV Higgs boson decays in the complex NMSSM,” *Phys.Rev.* **D89** (2014) 095013, [arXiv:1310.8129 \[hep-ph\]](#).
- [28] F. Domingo, “A New Tool for the study of the CP-violating NMSSM,” *JHEP* **06** (2015) 052, [arXiv:1503.07087 \[hep-ph\]](#).
- [29] T. Graf, R. Grober, M. Muhlleitner, H. Rzehak, and K. Walz, “Higgs Boson Masses in the Complex NMSSM at One-Loop Level,” *JHEP* **1210** (2012) 122, [arXiv:1206.6806 \[hep-ph\]](#).
- [30] M. Muhlleitner, D. T. Nhung, H. Rzehak, and K. Walz, “Two-loop contributions of the order  $\mathcal{O}(\alpha_t \alpha_s)$  to the masses of the Higgs bosons in the CP-violating NMSSM,” *JHEP* **05** (2015) 128, [arXiv:1412.0918 \[hep-ph\]](#).
- [31] CMS Collaboration, V. Khachatryan *et al.*, “Precise determination of the mass of the Higgs boson and tests of compatibility of its couplings with the standard model predictions using proton collisions at 7 and 8 TeV,” *Eur. Phys. J.* **C75** no. 5, (2015) 212, [arXiv:1412.8662 \[hep-ex\]](#).
- [32] ATLAS Collaboration, “Updated coupling measurements of the Higgs boson with the ATLAS detector using up to 25 fb<sup>-1</sup> of proton-proton collision data,” Tech. Rep. ATLAS-CONF-2014-009, CERN, Geneva, May, 2014.

- [33] J. Baglio, R. Grober, M. Muhlleitner, D. Nhung, H. Rzehak, *et al.*, “NMSSMCALC: A Program Package for the Calculation of Loop-Corrected Higgs Boson Masses and Decay Widths in the (Complex) NMSSM,” *Comput.Phys.Commun.* (2014), [arXiv:1312.4788 \[hep-ph\]](#).
- [34] ATLAS and CMS Collaborations, G. Aad *et al.*, “Combined Measurement of the Higgs:2012triggs Boson Mass in  $pp$  Collisions at  $\sqrt{s} = 7$  and 8 TeV with the ATLAS and CMS Experiments,” [arXiv:1503.07589 \[hep-ex\]](#).
- [35] P. Bechtle, S. Heinemeyer, O. Stal, T. Stefaniak, and G. Weiglein, “*HiggsSignals*: Confronting arbitrary Higgs sectors with measurements at the Tevatron and the LHC,” *Eur.Phys.J.* **C74** no. 2, (2014) 2711, [arXiv:1305.1933 \[hep-ph\]](#).
- [36] J. F. Gunion, Y. Jiang, and S. Kraml, “Diagnosing Degenerate Higgs Bosons at 125 GeV,” *Phys.Rev.Lett.* **110** (2013) 051801, [arXiv:1208.1817 \[hep-ph\]](#).
- [37] M. D. Goodsell, K. Nickel, and F. Staub, “Two-loop corrections to the Higgs masses in the NMSSM,” *Phys.Rev.* **D91** no. 3, (2015) 035021, [arXiv:1411.4665 \[hep-ph\]](#).
- [38] F. Staub, private communication.
- [39] F. Feroz and M. Hobson, “Multimodal nested sampling: an efficient and robust alternative to MCMC methods for astronomical data analysis,” *Mon.Not.Roy.Astron.Soc.* **384** (2008) 449, [arXiv:0704.3704 \[astro-ph\]](#); F. Feroz, M. Hobson, and M. Bridges, “MultiNest: an efficient and robust Bayesian inference tool for cosmology and particle physics,” *Mon.Not.Roy.Astron.Soc.* **398** (2009) 1601–1614, [arXiv:0809.3437 \[astro-ph\]](#); F. Feroz, M. Hobson, E. Cameron, and A. Pettitt, “Importance Nested Sampling and the MultiNest Algorithm,” [arXiv:1306.2144 \[astro-ph.IM\]](#).
- [40] P. Bechtle, O. Brein, S. Heinemeyer, G. Weiglein, and K. E. Williams, “HiggsBounds: Confronting Arbitrary Higgs Sectors with Exclusion Bounds from LEP and the Tevatron,” *Comput.Phys.Commun.* **181** (2010) 138–167, [arXiv:0811.4169 \[hep-ph\]](#); P. Bechtle, O. Brein, S. Heinemeyer, G. Weiglein, and K. E. Williams, “HiggsBounds 2.0.0: Confronting Neutral and Charged Higgs Sector Predictions with Exclusion Bounds from LEP and the Tevatron,” *Comput.Phys.Commun.* **182** (2011) 2605–2631, [arXiv:1102.1898 \[hep-ph\]](#); P. Bechtle, O. Brein, S. Heinemeyer, O. Stal, T. Stefaniak, *et al.*, “Recent Developments in HiggsBounds and a Preview of HiggsSignals,” *PoS CHARGED2012* (2012) 024, [arXiv:1301.2345 \[hep-ph\]](#); P. Bechtle, O. Brein, S. Heinemeyer, O. Stal, T. Stefaniak, *et al.*, “HiggsBounds – 4: Improved Tests of Extended Higgs Sectors against Exclusion Bounds from LEP, the Tevatron and the LHC,” *Eur.Phys.J.* **C74** (2014) 2693, [arXiv:1311.0055 \[hep-ph\]](#).
- [41] A. Djouadi, J. Kalinowski, and M. Spira, “HDECAY: A Program for Higgs boson decays in the standard model and its supersymmetric extension,” *Comput.Phys.Commun.* **108** (1998) 56–74, [arXiv:hep-ph/9704448 \[hep-ph\]](#).
- [42] B. Das, S. Moretti, S. Munir and P. Poulose, in preparation.